Proc. 2nd Symp. Smart Control of Turbulence, Mar. 2001, Tokyo, pp. 19-26

R&D Study on Micro Sensors and Actuators for Active Control of Wall Turbulence

Yuji SUZUKI, Nobuhide KASAGI, and Takashi YOSHINO
Department of Mechanical Engineering, The University of Tokyo, Hongo, Bunkyo-ku, Tokyo 113-8656

In order to a realize feedback control system of wall turbulence an R&D study of micro wall sensors and wall deformation actuators is now in progress. Micro hot-film sensors for the measurement of streamwise and spanwise wall shear stresses were developed and evaluated in a wind tunnel. Their dynamic response was much slower than the value previously estimated. Numerical analysis of the thermal field in the sensor chip shows that the heat loss to the substrate is very large even when an insulation air cavity is provided. As a prototype of wall deformation actuator, miniature electromagnetic actuators were fabricated. Although their dimension is somewhat larger than their ideal values, they offer a sufficient dynamic response and wall displacement. A preliminary experiment of an electrostrictive polymer actuator has been carried out successfully, and this new material seems promising for our next generation actuator.

1. Introduction

In the last decade, active feedback control of wall turbulence attracts much attention because of its potential to obtain large control effect with a small energy input. Since Choi et al. (1994) demonstrated that more than 20% drag reduction can be achieved by local blowing/suction with the aid of direct numerical simulation (hereafter, DNS) of turbulent channel flow, various control algorithms were proposed based on physical arguments of near-wall coherent structures, suboptimal/optimal control theories, and so on (e.g., Moin & Bewley, 1994; Gad-el-Hak, 1996; Kasagi, 1998). A number of previous studies reported substantial drag reduction in their DNS of wall turbulence, but experimental attempts are very limited (Tsao et al., 1997; Rathnasingham & Breuer, 1997), and no direct evidence of drag reduction has been obtained.

This is partially because the control algorithms are still not realistic to be applied to physical experiments, since an infinite number of sensors and actuators were assumed in most previous studies, and their volumes were neglected. A major difficulty also exists in the development of hardware; sensors and actuators should have spatio-temporal scales comparable to those of the near-wall coherent structures, which are generally very small and decreased with the Reynolds number. Recent development of microelectromechanical systems (MEMS) technology enables us to fabricate prototypes of micro devices (e.g., Ho & Tai, 1996). However, even in laboratory experiments, it is not straightforward to establish a feedback control system for wall turbulence, because a large number of sensors and actuators are required in order to obtain perceivable drag reduction.

The final goal of the present study is to develop a feedback control system for reducing turbulent skin friction and evaluate its performance in a laboratory experiment. In the present paper, development of prototype micro sensors and actuators are introduced, and preliminary evaluation of these devices are presented.

2. Smart Skin

Figure 1 shows a schematic of the “smart skin” for active feedback control of wall turbulence. Wall

sensors are employed to detect instantaneous flow information. Actuators should also be mounted flush on the wall and they are driven by a control signal from control units. Among various kinds of actuators, wall deformation is considered to be one of the most promising candidates, because they are robust against hostile environment.

Endo et al. (2000) assumed arrayed wall shear stress sensors and wall deformation actuators of finite spatial dimensions in their DNS. They developed a control algorithm based on the spanwise gradients of instantaneous wall shear stresses through physical arguments on near-wall coherent structures. They found that near-wall streamwise vortices are markedly attenuated, and about 10% drag reduction is obtained. Their results encourage us to develop a control system based on wall shear stress sensors and wall deformation actuators in our physical experiment.

Figure 2 shows a schematic of an air channel flow facility designed for the feedback control of wall turbulence. The channel width H and height were 50 and 500 mm, respectively. The test section is located $80H$ downstream from the inlet, where the flow is fully-developed. The bottom wall is equipped with a floating element (64x64 mm^2, Fig. 3), by which the skin friction is directly measured. Preliminary experiments to evaluate the measurement accuracy of the floating element is now undertaken. In the feedback control experiments, arrayed sensors and actuators as well as the control units will be installed in the floating element. The bulk mean velocity U_m is changed from 2.4 to 9.1 m/s, which corresponds to the Reynolds number Re_τ from 260 to 780. When U_m=7.5 m/s, the characteristic spatial and temporal scales of the near-wall streamwise vortices are respectively estimated to be 3 ms and 1 mm. Sensors and actuators should be designed in such a way that they satisfy these requirements.

3. Development of arrayed micro wall shear stress sensor

Up to now, various types of micro sensors were proposed for the measurement of the wall shear stress. Schmidt et al. (1988) developed a micro floating element having a sensing area of 500x500μm^2 by using the MEMS techniques. Naqwi & Reynolds (1991) made a novel shear stress sensor based on fan fringes using laser optics. In the present study, thermal sensor is adopted because its microfabrication process is relatively simple. Alfredsson et al. (1988) claimed that hot-film sensors suffer from heat conduction loss to the substrate, and that their frequency response should be deteriorated. Jiang et al. (1996) developed an array of micro hot-film shear stress sensors having 150 μm in length. They reported that the frequency response of their sensor is much improved when an insulating vacuum cavity is made underneath the hot-film. However, the bandwidth remains unclear, because direct evaluation of its response was not made.

Figure 4(a) shows one unit of the single sensor chip (Type 1, hereafter) developed in the present study. A thin film heater made of platinum is deposited on an 1μm-thick Si_3N_4 diaphragm. In order to keep the electric resistance of the hot-film sufficiently high, thin line of platinum film is patterned zigzag within an area of 200 × 23 μm^2. An air cavity of 200 μm in depth is formed underneath the hot-film by using anisotropic etching of the silicon substrate. The dimensions of the diaphragm is 400 × 400 μm^2. For Type 1, 8 sensors are fabricated per chip with an 1 mm spacing, and by attaching 6 chips on a print-circuit board aligned in the spanwise direction, an array of 48 sensors can be developed. It is noted that physical properties of the materials employed in the present sensors such as thermal capacity and heat conductivity are similar to those of Jiang et al. (1996), whilst they have a 2μm-thick vacuum cavity instead of the air cavity.

Figure 4(b) shows the dual sensor chip (Type 2, hereafter). Because the spanwise wall shear stress is very useful in detecting the near-wall coherent structures (e.g., Lee et al., 1998; Endo et al., 2000), Type 2 sensor is designed for simultaneous measurements of the streamwise and spanwise wall shear stresses. As shown in Fig. 4(b), two hot-films (300 × 32 μm^2), which are perpendicular to each other are deposited on diaphragms of 500 × 500 μm^2 in area. The spacing between the center of two hot-films is 530 μm, while the spanwise spacing between neighboring sensors is 2 mm.

Each hot-film is driven as a constant temperature anemometer and kept about 60 °C higher than the ambient temperature. The streamwise gradient of the static wall pressure was employed for the sensor calibration, and a third-order polynomial of the bridge voltage squared was used as the fitting function. For Type 2, a modified cosine law is assumed for the dependency of the cooling velocity on the angle of attack.

The spanwise two-point correlation of τ_w obtained with the arrayed sensor (Fig. 4c) is shown in Fig. 5. The present data of $R_{\tau w \tau w}$ are mostly in accordance with the DNS data. Thus, the near-wall coherent structures, which are the target for the feedback control, can be captured with the present wall shear stress sensors. Although it is now shown here, the rms values of the streamwise and spanwise wall shear stresses measured are in accordance with the DNS data, but the deviation over the DNS data is increased with the Reynolds number because of the imperfect dynamic response of the sensor.

Figure 6 shows the power spectrum of the streamwise shear stress at Re_τ=341 measured with the Type 2 sensor. In this particular measurement, the sensor chip was mounted in such a way that one of the hot-films is perpendicular to the streamwise direction. The frequency is non-dimensionalized with the wall friction velocity and the kinematic viscosity. The non-dimensional frequency corresponding to the reciprocal of the Kolmogorov's time scale estimated is 0.47. The power spectra presently obtained are in good agreement with the DNS data of Iwamoto et al. (2001) at $f^+ < 0.04$ ($f < 120$ Hz), while the gain is decreased at the higher frequencies. Jiang et al. (1996) reported that their shear stress sensor has a bandwidth of 10kHz. However, their estimates should be erroneous, since the structure and materials of their sensor are similar to ours as mentioned above.

In order to design shear stress sensor having better frequency response, heat transfer analysis using a numerical simulation is made. In our first stage, a two-dimensional model shown in Fig. 7 was investigated, and the effect of air cavity was examined. The fluid velocity was given with a linear function of the distance to the wall in order to mimic the velocity distribution inside the viscous sublayer. A control volume method is employed for the spatial discretization of the energy equation, and a fully-implicit method was used for the temporal discretization. In the present computation, the temperature of the hot-film is kept constant, which corresponds to an assumption that the constant temperature circuit has an ideal response.

Figure 8 shows contours of temperature when steady wall shear corresponding to Re_τ=341 is applied. For the conventional sensor, in which the hot-film is directly attached to the epoxy substrate, contours spread widely in all directions, and the heat loss to the substrate is about 98% of the total heat generated in the hot-film. On the other hand, for the present sensor having an insulating air cavity in a silicone substrate, the heat loss is decreased by 50%, and the temperature gradient is almost concentrated in the diaphragm and the air cavity. Figure 9 shows the dynamic response of the sensor to sinusoidally oscillated wall shear. As expected, the sensor presently employed is superior in the gain characteristics to the conventional sensor. However, the gain of the present sensor is also decreased rapidly with increasing frequency, and about 0.55 at f=100Hz. This numerical result is in accordance with the present experimental data shown in Fig. 6. It is noted that about 65% of the heat loss is due to the tangential heat conduction in the diaphragm even when an insulation layer is provided. Therefore, in order to design hot-film shear stress sensor having higher bandwidth, more sophisticated design should be required.

4. Development of arrayed wall deformation actuator

For micro actuators, various characteristics such as large strain, fast response, and low energy consumption are simultaneously needed in practical applications. Although a number of actuation principles such as electrostatic, electromagnetic, and piezoelectric have been proposed, none of them can satisfy all these requirements. Therefore, in the present study, we are aiming at two somewhat different approaches in order to establish the micro arrayed actuators. One direction is to develop micro actuators by using an actuation principle readily available and make a leading design of the whole feedback control system. In this

context, we adopt electromagnetic actuator, of which defect is its large energy consumption. Another direction is to attack a new promising actuation principle and establish its design rule and the microfabrication techniques. We choose electrostrictive polymer actuator for this purpose, since it will provide very large strain and high frequency response with a potential for low energy consumption (Pelrine et al., 1998).

Figure 10 shows a prototype of electromagnetic wall deformation actuator. Silicone rubber on the top having 0.1 mm in thickness is deformed by the magnetic force between a rare-earth miniature permanent magnet and a small copper coil. The outer diameter is 3 mm (100 wall units), and the spanwise spacing between neighboring actuators is 6 mm. Thus, its dimensions are somewhat larger than the requirement in our laboratory experiment mentioned above. By applying 100mA current to the coil, about 100 μm deformation was obtained. Figure 11 shows the dynamic response of the actuator. The resonant frequency is about 640 Hz, so that the bandwidth of this prototype should be sufficient. Currently, preliminary experiments using arrayed actuators are undertaken. The effect of actuator motion on the turbulent structures will be evaluated in the turbulent channel flow. Figure 12 shows a schematic of microfabricated actuator for our next generation actuator. Fabrication process of multilayered coil and polymer magnet is now investigated.

Electrostriction using polymer elastomers is relatively new for micro actuation principle. Figure 13 shows the relation between strain and actuation pressure per unit mass (Pelrine et al., 1998). Electromagnetic and electrostatic actuators achieve large strain, but their relative actuation pressure is small. On the other hand, piezoelectric actuator has large actuation pressure, but its strain is much less than 1 %. On the other hand, the electrostrictive polymer actuator has good performance in both parameters. Recently, Pelrine et al. (2000) demonstrated that more than 100 % strain can be achieved with this type of actuator.

Figure 14 shows the operation principle of electrostrictive polymer actuator. When a voltage difference is applied between the two compliant electrodes, the polymer in between is squeezed in thickness and stretched in the horizontal direction due to the electrostatic force between the electrodes. The effective pressure between the electrodes is proportional to the permittivity of the polymer and the electric field squared (Pelrine et al., 1998). One possible defect of the electrostrictive polymer actuator is that it requires high electric field (>30V/μm). Thus, a thin polymer film of a few μm should be employed for practical use.

Figure 15 shows a schematic of a flap actuator for evaluating various polymer materials and electrodes. Conductive silicone is employed for the compliant electrodes. The deformation of the flap is measured with a laser displacement measurement system (Fig. 16). As shown in Fig. 17, the deformation depends on the electric field squared as expected, and 800 μm displacement is obtained for RTV8600 (Dow Corning Corp.) at 30V/μm. Further tests are now undertaken to determine the physical quantities of the polymer film. Optimal design of the wall deformation actuator shown in Fig. 18 will be made with the aid of a mathematical model.

5. Conclusions

R&D studies for the development of arrayed micro shear stress sensors and wall deformation actuators were made. Hot-film sensors for the measurement of the streamwise and spanwise wall shear stresses were developed. The dynamic response of the thermal sensor was evaluated through physical experiment and numerical analysis. It is found that the bandwidth is much lower than the value previously estimated. More sophisticated design should be required in order to improve its performance. As a prototype of wall deformation actuator, miniature electromagnetic actuator was fabricated. Although its dimensions are somewhat larger than its required values, it provides sufficient dynamic response and wall displacement. A preliminary experiment of an electrostrictive polymer actuator has also been carried out successfully, and this new material seems promising for our next generation actuator.

The authors are grateful to Mr. S. Kamiunten in Yamatake Corp. for his corporation in manufacturing

micro shear stress sensors. The authors also thank to Messrs. M. Tsuda, M. Murakami and H. Tsutsui for their aids in their laboratory work.

References

Alfredsson, P. H., Johansson, A. V., Haritonidis, J. H., and Eckelmann, H., 1988, Phys. Fluids, 31, 1026.
Choi, H., Moin, P., and Kim, J., 1994, J. Fluid Mech., 262, 75-110.
Endo, T., Kasagi, N., and Suzuki, Y., 2000, Int. J. Heat Fluid Flow, 21, 568.
Gad-el-Hak, M., 1996, Appl. Mech. Rev., 49, 377.
Ho, C. M., and Tai, Y. C., 1996, ASME J. Fluids Eng. 118, 437.
Iwamoto, K., Suzuki, Y., and Kasagi, N., 2001, 2nd Int. Symp. Turbulence and Shear Flow Phenomena, Stockholm, to be presented.
Jiang, F., Tai, Y.-C., Gupta, B., Goodman, R., Tung, S., Huang, J.-B., and Ho, C.-M., 1996, Proc. IEEE Workshop on MEMS, 110.
Kasagi, N., 1998, Int. J. Heat & Fluid Flow, 19, 134.
Kim, J., Moin, P., and Moser, R., 1987, J. Fluid Mech., 177, 133.
Kuroda, A., Kasagi, N., and Hirata, M., 1995, Turbulent Shear Flows IX, F. Durst et al., eds., Springer-Verlag, Berlin, 241.
Lee, C., Kim, J., and Choi, H., 1998, J. Fluid Mech., 358, 245.
Moin, P., and Bewley, T., 1994, Appl. Mech. Rev., 47, S3.
Moser, R. D., Kim, J., and Mansour, N. N., 1999, Phys. Fluids, 11, 943.
Rathnasingham, R., and Breuer, K. S., 1997, Phys. Fluids, 9, 1867.
Pelrine, R., Kornbluh, R. D., and Joseph, J. P., 1998, Sensors Actuators, A PHys., 64, 77.
Pelrine, R., Kornbluh, R. D., Pei, Q., and Joseph, J. P., 2000, Science, 287, 836.
Schmidt, M. A., Howe, R. T., Senturia, S. D., and Haritonidis, J. H., 1988, IEEE Trans. ED-35, 750.
Tsao, T., Jiang, F., Miller, R. A., Tai, Y. C., Gupta, B., Goodman, R., Tung, S., and Ho, C. M., 1997, Technical Digest, Transducers '97, Chicago, 1, 315-318.

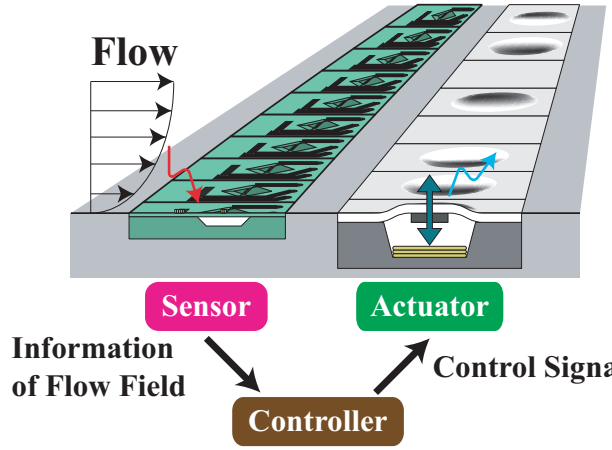

Fig. 1 Schematic diagram of active feedback control system for wall turbulence.

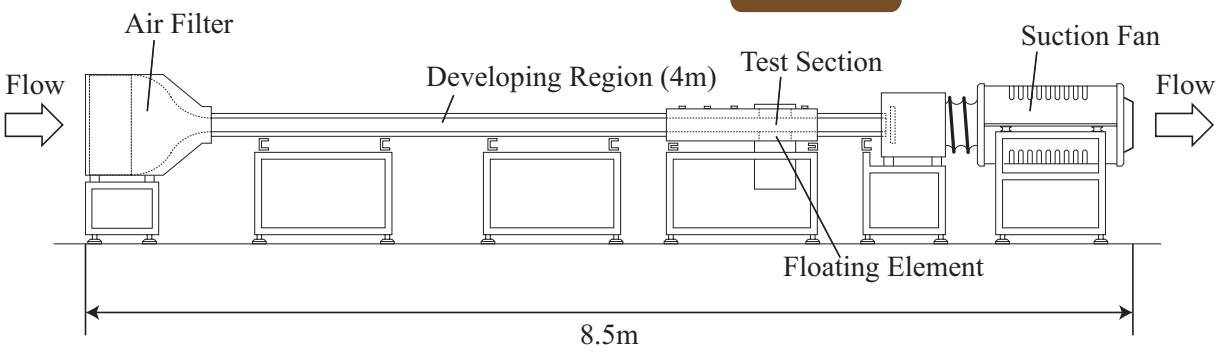

Fig. 2 Schematic diagram of a turbulent air channel flow facility for active feedback control.

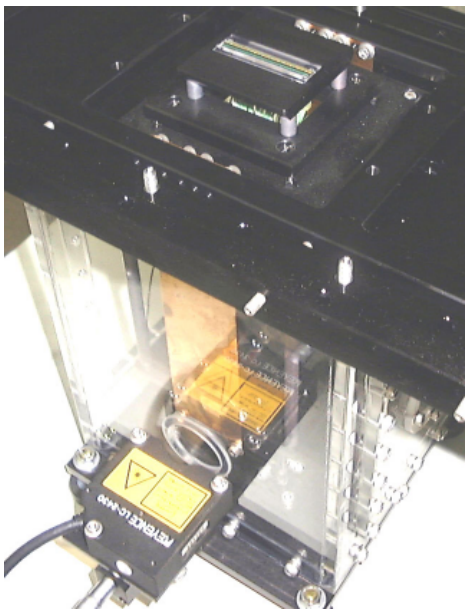

Fig. 3 Floating element setup.

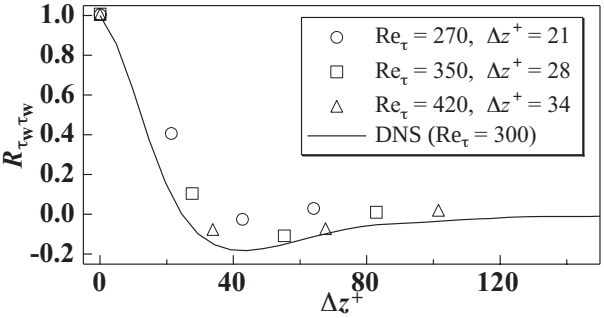

Fig. 5 Spanwise two-point correlations of the spanwise shear stress fluctuation.

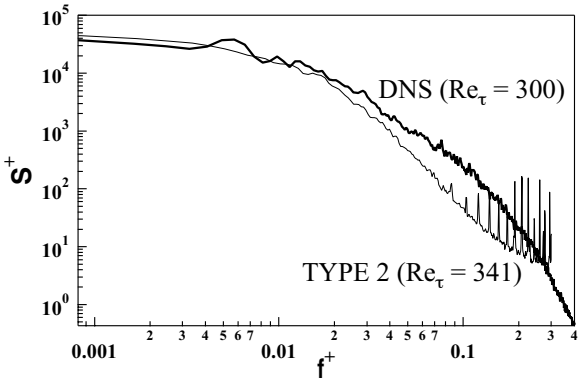

Fig. 6 Power spectra of the streamwise wall shear stress measured with Type 2.

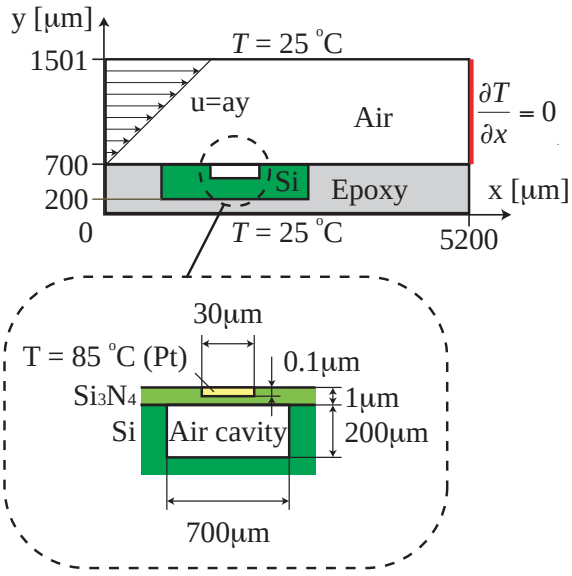

Fig. 7 Computational model.

Fig. 4 Micro hot-film shear stress sensor. (a) Magnified view of a single sensor chip (Type 1), (b) Magnified view of a dual sensor chip (Type2), (c) Arrayed shear stress sensor.

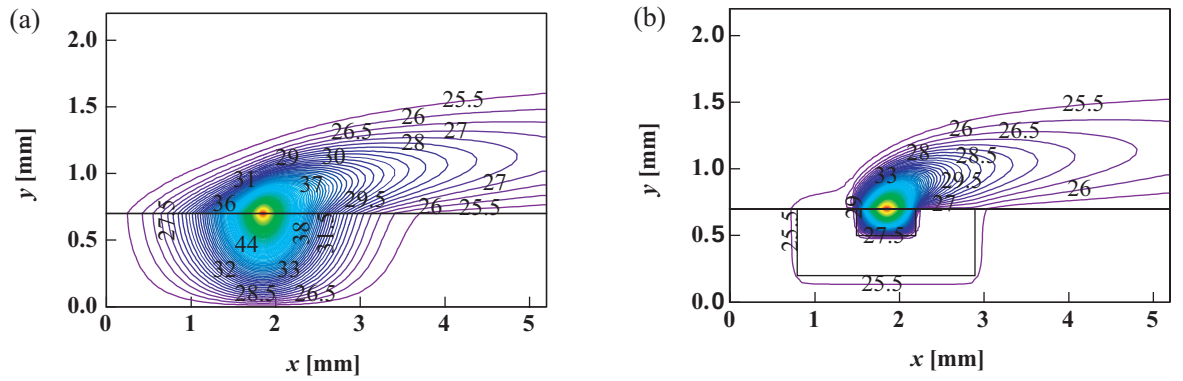

Fig. 8 Temperature distribution. (a) Conventional sensor, (b) Sensor having an insulation air cavity.

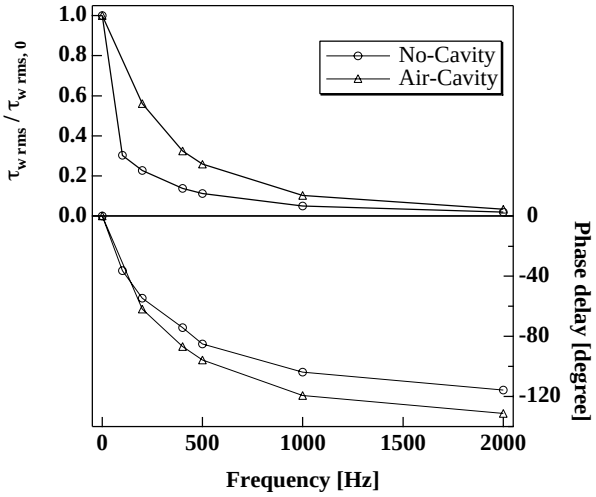

Fig. 9 Dynamic response of the sensor model.

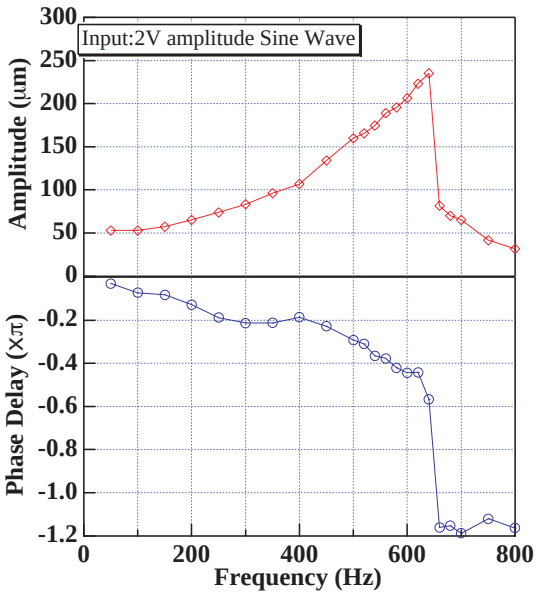

Fig. 11 Dynamic response of electromagnetic wall deformation actuator.

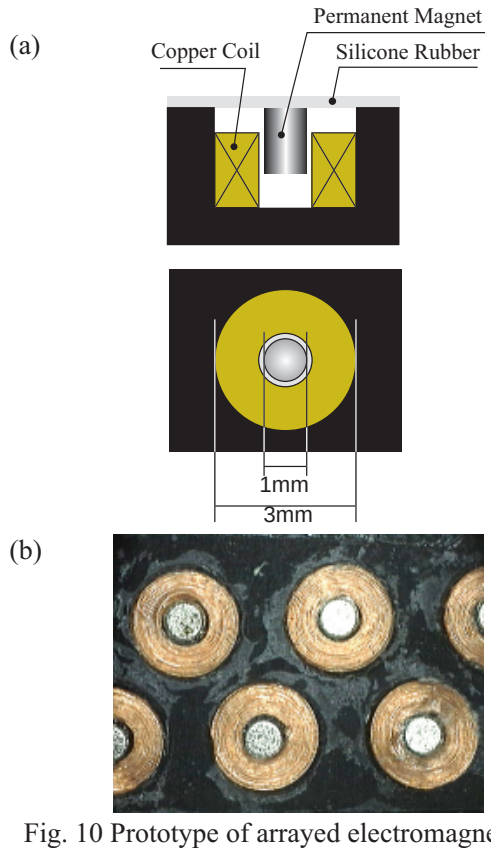

Fig. 10 Prototype of arrayed electromagnetic wall deformation actuator. (a) Schematic diagram, (b) Top view.

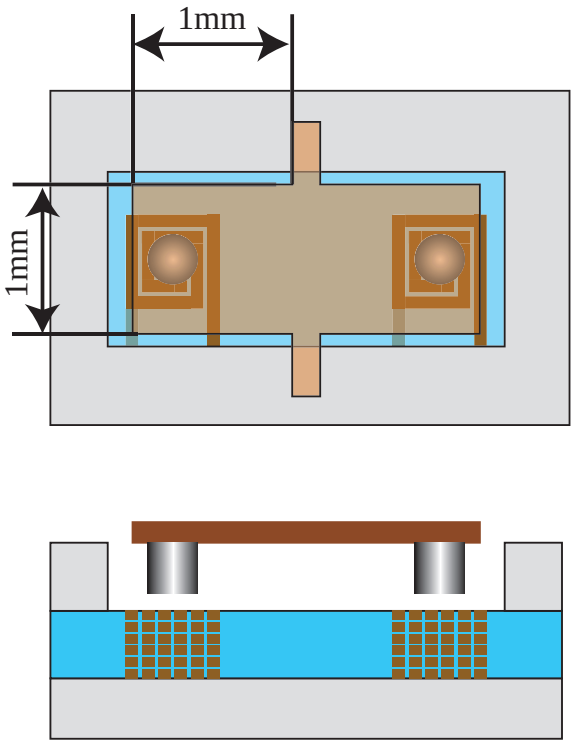

Fig. 12 Micro-fabricated electromagnetic actuator.

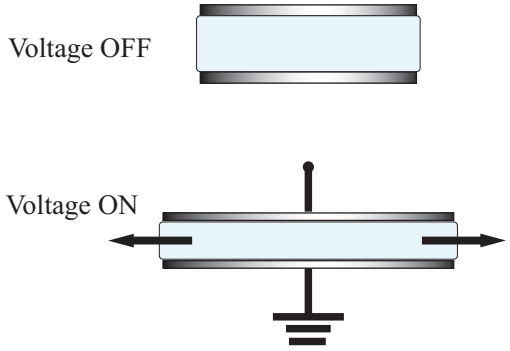

Fig. 13 Operation principle of electrostrictive polymer actuator.

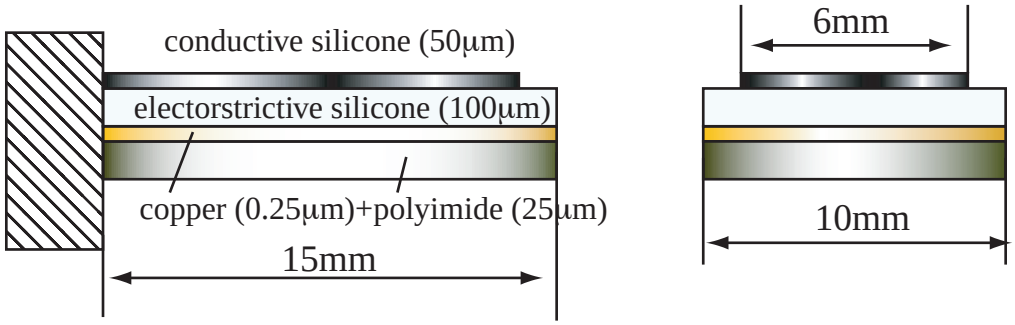

Fig. 14 Schematic diagram of the electrostrictive polymer flap actuator for a preliminary experiment.

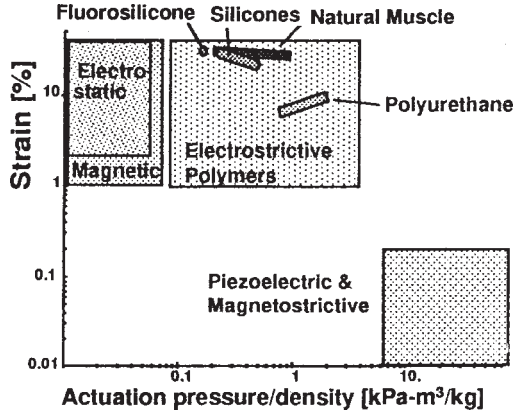

Fig. 15 Comparison of high-speed technologies (by Pelrine et al., 1998).

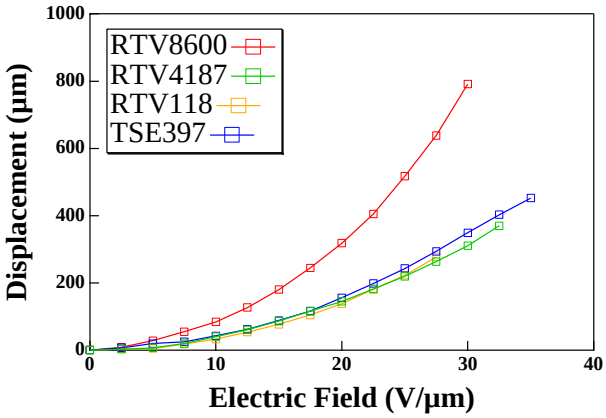

Fig. 17 Deformation of the flap actuator versus the electric field imposed.

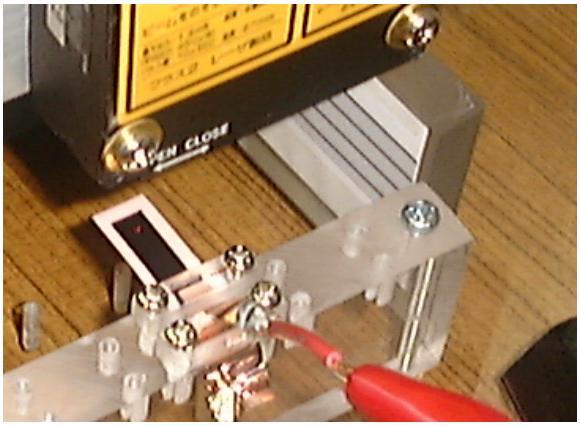

Fig. 16 Preliminary measurement setup for evaluating static response of electrostrictive polymer actuator.

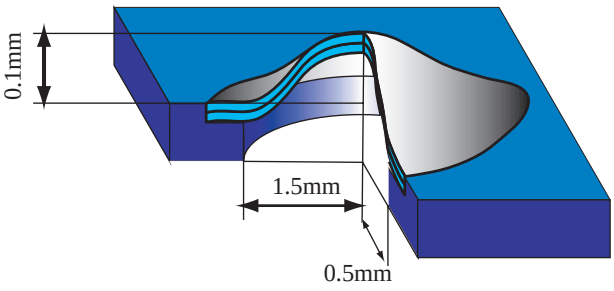

Fig. 18 Schematic diagram of the electrostrictive wall deformation actuator